



## Cusp and Nightside Auroral Sources of $O^+$ in the Plasma Sheet

L. Kistler, C. Mouikis, K. Asamura, S. Yokota, S. Kasahara, Y. Miyoshi, K. Keika, A. Matsuoka, I. Shinohara, T. Hori, et al.

### ► To cite this version:

L. Kistler, C. Mouikis, K. Asamura, S. Yokota, S. Kasahara, et al.. Cusp and Nightside Auroral Sources of  $O^+$  in the Plasma Sheet. *Journal of Geophysical Research Space Physics*, 2019, 124 (12), pp.10036-10047. 10.1029/2019JA027061 . hal-03016825

**HAL Id: hal-03016825**

**<https://hal.science/hal-03016825>**

Submitted on 23 Nov 2020

**HAL** is a multi-disciplinary open access archive for the deposit and dissemination of scientific research documents, whether they are published or not. The documents may come from teaching and research institutions in France or abroad, or from public or private research centers.

L'archive ouverte pluridisciplinaire **HAL**, est destinée au dépôt et à la diffusion de documents scientifiques de niveau recherche, publiés ou non, émanant des établissements d'enseignement et de recherche français ou étrangers, des laboratoires publics ou privés.

# JGR Space Physics

## RESEARCH ARTICLE

10.1029/2019JA027061

### Key Points:

- Arase and MMS are fortuitously located in the near-Earth and midtail plasma sheet boundary layer during the main phase of a storm
- Both spacecraft observe  $O^+$  from both the nightside aurora and the cusp, with higher energies observed at greater distances
- The energy differences and timing of the  $O^+$  at the two spacecraft are consistent with modeled transport

### Correspondence to:

L. M. Kistler,  
lynn.kistler@unh.edu

### Citation:

Kistler, L. M., Mouikis, C. G., Asamura, K., Yokota, S., Kasahara, S., Miyoshi, Y., et al. (2019). Cusp and nightside auroral sources of  $O^+$  in the plasma sheet. *Journal of Geophysical Research: Space Physics*, 124, 10,036–10,047. <https://doi.org/10.1029/2019JA027061>















Received 21 JUN 2019

Accepted 15 OCT 2019

Accepted article online 7 NOV 2019

Published online 09 DEC 2019

## Cusp and Nightside Auroral Sources of $O^+$ in the Plasma Sheet

L. M. Kistler<sup>1,2</sup> , C. G. Mouikis<sup>1</sup> , K. Asamura<sup>3</sup> , S. Yokota<sup>4</sup> , S. Kasahara<sup>5</sup> , Y. Miyoshi<sup>2</sup> , K. Keika<sup>5</sup> , A. Matsuoka<sup>3</sup> , I. Shinohara<sup>3</sup> , T. Hori<sup>2</sup> , N. Kitamura<sup>5</sup> , S. M. Petrinec<sup>6</sup> , I. J. Cohen<sup>7</sup> , and D. C. Delcourt<sup>8</sup> 

<sup>1</sup>Space Science Center, University of New Hampshire, Durham, NH, USA, <sup>2</sup>Institute for Space Earth Environmental Research, Nagoya, Japan, <sup>3</sup>ISAS, JAXA, Sagami-hara, Japan, <sup>4</sup>Graduate School of Science, Osaka University, Toyonaka, Japan, <sup>5</sup>Department of Earth and Planetary Science, Graduate School of Science, University of Tokyo, Tokyo, Japan, <sup>6</sup>Lockheed Martin Advanced Technology Center, Palo Alto, CA, USA, <sup>7</sup>The Johns Hopkins University Applied Physics Laboratory, Laurel, MD, USA, <sup>8</sup>Laboratoire de Physique des Plasmas, Sorbonne Université, Paris, France

**Abstract** Energetic  $O^+$  outflow is observed from both the dayside cusp and the nightside aurora, but the relative importance of these regions in populating the plasma sheet and ring current is not known. During a storm on 16 July 2017, the Arase and MMS satellites were located in the near-Earth and midtail plasma sheet boundary layers (PSBL). During the storm main phase, Arase and MMS both observe  $O^+$  in the lobe entering the PSBL, followed by a time period with energy-dispersed bursts of tailward-streaming  $O^+$ . The ions at MMS are at higher energies than at Arase. Trajectory modeling shows that the ions coming in from the lobe are cusp origin, while the more energetic bursty ions are from the nightside aurora. The observed and simulated energies and temporal dispersion are consistent with these sources. Thus, both regions directly contribute  $O^+$  to the plasma sheet during this storm main phase.

**Plain Language Summary** The magnetosphere is the region of space encompassed by Earth's magnetic field. The plasma trapped in the magnetosphere can come both from the Sun and from the ionosphere, the ionized layer of the atmosphere. The ionospheric contribution to the plasma increases during geomagnetic storms. These ions get energized in the auroral oval and flow out along magnetic field lines. During storms, this outflow can contain a large fraction of  $O^+$ . There are two particular regions where this  $O^+$  outflow occurs, one on the dayside and one on the nightside. This study looks at the contribution of  $O^+$  from these two regions. Two spacecraft in different locations in the magnetosphere during the storm were able to observe the signatures of ions from both regions indicating that both regions are important during the peak of the storm.

## 1. Introduction

There are two main regions where energetic ( $>100$  eV)  $O^+$  outflow is observed: the cusp and the nightside aurora. The processes leading to this ion outflow and the outflow characteristics have been recently reviewed by Maggiolo (2016). Ions are accelerated from both regions by a two-step process. Solar EUV is the primary source of ionization and heating of the ionosphere, but in the auroral zone, the solar wind-magnetosphere coupling drives additional energy into the ionosphere through both particle precipitation and electromagnetic Poynting flux that provides the additional heating that leads to ion upflow. At higher altitudes, both transverse ion acceleration due to wave particle interactions and parallel acceleration due to quasi-static electric fields further accelerate the ions, allowing them to escape into the magnetosphere. While the various mechanisms that accelerate ions can occur in both regions, the drivers vary with local time, and so the timing of the outflow and the energies reached can be different in the two regions. In the cusp, the energy input comes from the direct interaction with the solar wind. Cusp outflow is enhanced by solar wind dynamic pressure (Fuselier et al., 2002; Moore et al., 1999), as well as with the solar wind electric field (Cully et al., 2003). Thus, increased cusp outflow may occur when a solar wind pressure enhancement reaches the Earth prior to a storm main phase as well as during the main phase. For the nightside aurora, the precipitation comes predominantly from the plasma sheet and plasma sheet boundary layer. Nightside outflow is strongly correlated with substorm activity and increases significantly during storm times (Wilson et al., 2004). In general, the cusp outflow number flux exceeds the nightside outflow (Cully et al., 2003; Peterson

et al., 2008), while the nightside outflow has higher energies (Andersson et al., 2005). While the characteristic energy of the outflow is relatively low,  $\sim 30$  eV in the cusp and  $\sim 50$  eV in the nightside aurora at 4,000 km (Andersson et al., 2005), the tail of the spectrum can extend to more than a keV. Auroral beams, which are caused by the quasi-static electric fields, can have energies approaching 10 keV (Collin et al., 1987; Möbius et al., 1998) while the conic distributions, caused by transverse acceleration, tend to be less than a keV (Tung et al., 2001). Clearly, both the cusp and the nightside auroral outflow are strong during storms, but the timing and characteristics of the two outflow sources may differ, and so the contributions of both to the magnetospheric population need to be considered.

Both the cusp and the nightside aurora can supply ions to the plasma sheet. From the cusp, ions move over the polar caps and enter the plasma sheet through the lobes. The  $O^+$  ion streams in the lobe have been observed and well characterized with the International Sun/Earth Explorer-2 (ISEE-2; Candidi et al., 1982), Geotail (Mukai et al., 1994), Polar (Liemohn et al., 2005), and Cluster (Liao et al., 2010). Their observed energy increases with distance from the neutral sheet and distance down the tail. During storms, their flux increases, and they are observed continuously from the cusp to the lobes and then entering the plasma sheet for many hours (Kistler et al., 2010). When they enter the plasma sheet, they are accelerated and heated (Hirahara et al., 1994; Orsini et al., 1990). The source of the acceleration and heating has not been definitely established. In some cases it is completely consistent with the enhanced  $E \times B$  drift under the convection electric field as the ion moves toward the neutral sheet, but there are also arguments for more local effects. Lindstedt et al. (2010) argued that the acceleration was due to a localized electric field at the boundary, and Lennartsson (2003) proposed that the localized electric fields could be due to the difference in gyro-radius between protons and electrons at the boundary.

As discussed above, nightside auroral outflow can also occur at all times, with an intensity that varies both with substorms and storms (Wilson et al., 2004). Nosé et al. (2016) has shown that for the L range from 4.5 to 6.6, 80% of nightside dipolarizations are accompanied by bursts of  $O^+$  that exhibit an energy dispersion consistent with their flight time from the ionosphere, indicating that most substorms result in enhanced ion outflow. Kistler et al. (2016) showed examples of this energy dispersed outflow at Van Allen Probes apogee during the storm main phase. However, the number of reported observations of these ions reaching the more distant plasma sheet is limited. Sauvaud et al. (2004) reported two examples from Cluster of “injections” at 17–19 Re. The ions were observed as strongly field aligned, energy dispersed structures, and a timing analysis showed that the dispersion was consistent with a time-of-flight effect with an origin at the nightside aurora. In these cases, the injections provided a large fraction (80%) of the  $O^+$  observed. Lund et al. (2018) examined the Cluster database of large storm-time substorms associated with sawtooth events, and found that only 2 out of 33 events showed  $O^+$  with the energy dispersion characteristic of the nightside auroral source. The other events showed features that were more consistent with  $O^+$  from the lobes entering the plasma sheet. Other observations (e.g., Daglis & Axford, 1996; Gazey et al., 1996) showed the fast appearance of energetic ( $>30$  keV) oxygen in the plasma sheet, but did not observe the actual injection itself, and so the origin could have been from the nightside aurora, but could also have been from the cusp. Thus, how often the nightside outflow reaches downtail beyond geosynchronous orbit is not known.

How far downtail the  $O^+$  reaches the equatorial plasma sheet is critical in determining its ultimate fate and impact. Modeling has shown that the further down the tail the ions enter the plasma sheet, the more they are energized in their earthward transport (e.g., Chappell et al., 2008). When the  $O^+$  ions enter the plasma sheet where the neutral sheet is thin, the  $O^+$  ions scatter and isotropize as they cross it, and can move cross-tail in the direction of the electric field, gaining energy. When the  $O^+$  ions enter closer to the Earth, where the field is more dipolar, their motion can remain adiabatic and the  $O^+$  ions can bounce and drift, only gaining energy proportional to the change in magnetic field, conserving their magnetic moment (Delcourt et al., 1988). At 15–19 Re, the location where the Cluster satellites normally cross the plasma sheet, the cusp ions are clearly observed entering the plasma sheet far enough down the tail to become isotropized and heated, becoming part of the hot plasma sheet (Kistler et al., 2010), but how often the auroral ions reach this far is not known. It has also been found that there is a significant radial gradient in the  $O^+/H^+$  ratio, with the ratio decreasing by a factor of 5 between  $L = 6.6$  and  $L = 15$  (Maggiolo & Kistler, 2014). Thus, there is significant additional  $O^+$  entering the plasmasheet between 6.6 and 15 Re, but it is not known if this is from the cusp or the nightside aurora.

The ring current is the population of particles that contributes the most to the energy density, or pressure, in the inner magnetosphere. The dominant energy range contributing to the ring current during storm times is from  $\sim 10$  to  $\sim 200$  keV (Williams, 1981). Kistler et al. (2016) used Van Allen Probes data during one storm to determine which source was more important in populating the ring current. They found that the population that contributed the most to the ring current  $O^+$  was the hot, more isotropic component of the plasma sheet, the population above  $\sim 5$  keV, not the lower energy, less than 1 keV, ions observed coming directly from the nightside aurora. Because this higher-energy  $O^+$  population increased prior to the storm main phase in this storm, after a large-pressure pulse had hit the Earth's magnetosphere but before there was a large increase in auroral activity, it was inferred that the cusp was the source for this enhanced  $O^+$ . However, because the direct entry of the cusp ions was not observed in this case, it cannot be excluded that the nightside auroral ions were getting far enough downtail prior to the storm to also scatter, and become part of the hot, isotropic component. Thus, more studies determining where and when the nightside auroral ions are able to reach further down the magnetotail are required.

In this paper, we examine an event where two spacecraft were fortuitously located in the plasma sheet boundary layer in the region between 6.6 and 15 Re during the main phase of a storm so that the input of the two sources to the plasma sheet as a function of radial distance can be observed.

## 2. Instrumentation

The ERG (Arase) satellite was launched in December 2016 into a  $31^\circ$  inclination orbit with apogee altitude of  $\sim 32,000$  km and perigee altitude of  $\sim 400$  km (Miyoshi et al., 2018). The satellite is well instrumented to measure the full particle and wave populations in the inner magnetosphere. In this paper, we concentrate on measurements of ion composition using both the Low Energy Particle Experiments-ion mass analyser (LEPi; Asamura et al., 2018) and the Medium-energy particle experiments-ion mass analyzer (MEPi; Yokota et al., 2017). LEPi and MEPi both measure 3-D distribution functions of the major ion species,  $H^+$ ,  $He^{++}$ ,  $He^+$ ,  $O^{++}$ ,  $O^+$ , and molecular ions, with LEPi covering the energy range  $<0.1$  to 25 keV/q, and MEPi covering the range from 10 to 180 keV/q. The Magnetic Field Experiment (MGF) data are used for determining pitch angle distributions (Matsuoka et al., 2018).

The Magnetospheric MultiScale (MMS) satellites are in a  $28.5^\circ$  inclination orbit with a low perigee (1.2 Re) and an apogee that depends on the phase. During the time period discussed in this paper, the spacecraft was in “phase 2b,” with an apogee of 25 Re. The MMS satellites are also well instrumented to measure 3-D distributions of the major ion species, with the Hot Plasma Composition Analyzer (HPCA) instrument (Young et al., 2014) covering energies from  $\sim 1$  eV to 40 keV, and the Energetic Ion Spectrometer (EIS; Mauk et al., 2016) measuring  $H^+$  above  $\sim 15$  keV and oxygen above 130 keV. The MMS data in this paper are all from MMS-2.

## 3. Observations

Figure 1 shows the orbits of the MMS and Arase satellites from 6:00 to 12:00 UT on 16 July 2017. The top panels show the  $x$ - $y$  and  $x$ - $z$  projections of the orbit in GSM coordinates. MMS was located on the dawnside of the magnetotail, and during this time moved earthward from  $x_{\text{gsm}}$  of 16 to 10. The Arase satellite moved outbound from dusk, across midnight, and then inbound on the dawn side. The  $x$ - $z$  projection shows that both spacecraft were at high latitudes. The bottom panel shows the  $x$ - $z$  projection along with field lines from a T89 (Tsyganenko, 1989) magnetic field for  $Kp = 6$ . Both spacecraft are well above the neutral sheet, close to the PSBL.

Figure 2 shows MMS-2 and Arase data, along with the solar wind parameters, from this time period. The solar wind parameters, from the OMNI database, have been propagated to the bow shock location. Figures 2a–2c show the solar wind dynamic pressure, the  $z$  component of the interplanetary magnetic field (IMF), and the  $SYM-H$  index. A strong pressure enhancement, followed by a southward turning of the IMF, drove a moderate geomagnetic storm. There is unfortunately a data gap in the solar wind pressure measurement just when the enhancement hits, but the timing of the enhancement hitting the Earth is clearly identified by the sharp increase in the  $SYM-H$  index. This index shows a strong increase when the pressure pulse hits, and then a decrease for the next 8 hr, indicating the main phase of the storm. The  $Dst$  index (not shown)

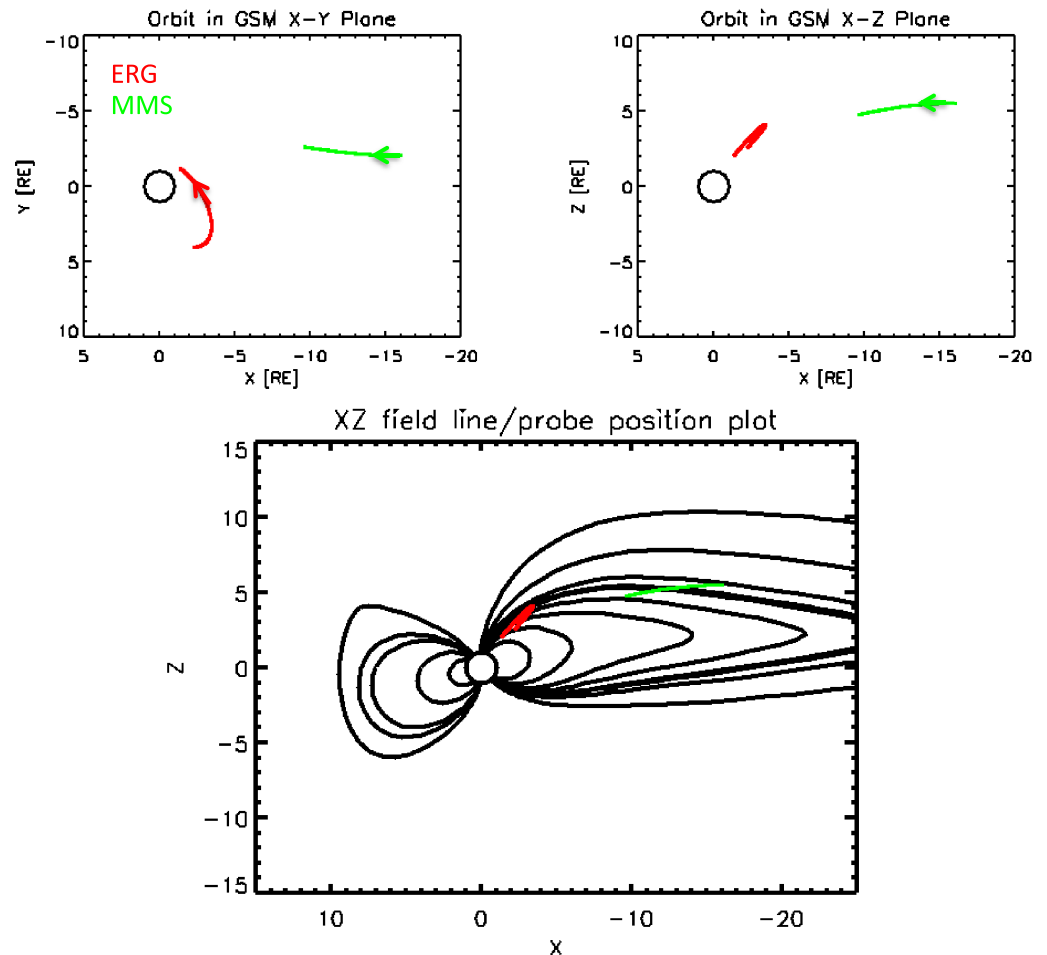


**Figure 1.** Orbits of the ERG spacecraft (red) and the MMS 2 spacecraft (green) for the time period from 6:00 to 12:00 on 16 July 2017. The top two panels show the projects into the x-y and x-z GSM plane, and the bottom panel shows the orbits projected onto a Tsyganenko T89  $K_p = 6$  magnetic field.

reached a minimum of  $-72$  nT at 15:00. Figure 2d shows the plasma beta on MMS. This gives a good indication when the spacecraft is in the plasma sheet ( $\beta > 0.1$ ) and when it is in the lobe ( $\beta < 0.1$ ). MMS starts in the lobe, and enters the plasma sheet at 6:25, after the pressure pulse hits. Figures 2e and 2f show the  $H^+$  data from EIS and HPCA on MMS. When MMS is in the lobe prior to 6:25, a low-energy narrow-energy  $H^+$  population is observed at  $\sim 20$  eV. After the dynamic pressure pulse hits, the spacecraft moves into the plasma sheet, and enhanced  $H^+$  is observed from  $\sim 100$  eV up to  $\sim 500$  keV. Figures 2g and 2h show the oxygen at MMS. Only a few oxygen counts are observed in the lobe prior to the pressure pulse. Then, when MMS enters the plasma sheet, first the energetic oxygen is observed. Then, when the spacecraft is closer to the plasma sheet boundary layer (PSBL), as indicated by the decreasing beta, a separate population of  $O^+$  just below 1 keV is observed, starting at  $\sim 7:20$ . This population continues, while decreasing in energy, when the spacecraft moves into the lobe at  $\sim 8:27$ . The energetic  $O^+$  is absent during this time, but a diffuse  $H^+$  population is still present in the lobe. When the spacecraft re-enters the PSBL at 9:38, a population with a broader energy distribution is observed. There is a final lobe excursion from 11:04 to 11:17. Then the spacecraft re-enters the plasma sheet.

Figures 2i and 2j show  $H^+$  from the Arase satellite. Arase is on an outbound pass at the start of the time period. Typical inner magnetosphere quiet-time energy spectra are observed on the outbound pass. When the pressure enhancement hits, there is an initial enhancement above 10 keV, likely due to the compression. At 6:20 an energy dispersed enhancement is observed, starting at the highest energies, and then decreasing. At 7:36, the  $H^+$  spectrum changes, as the spacecraft moves closer to the boundary layer. It enters the lobe at

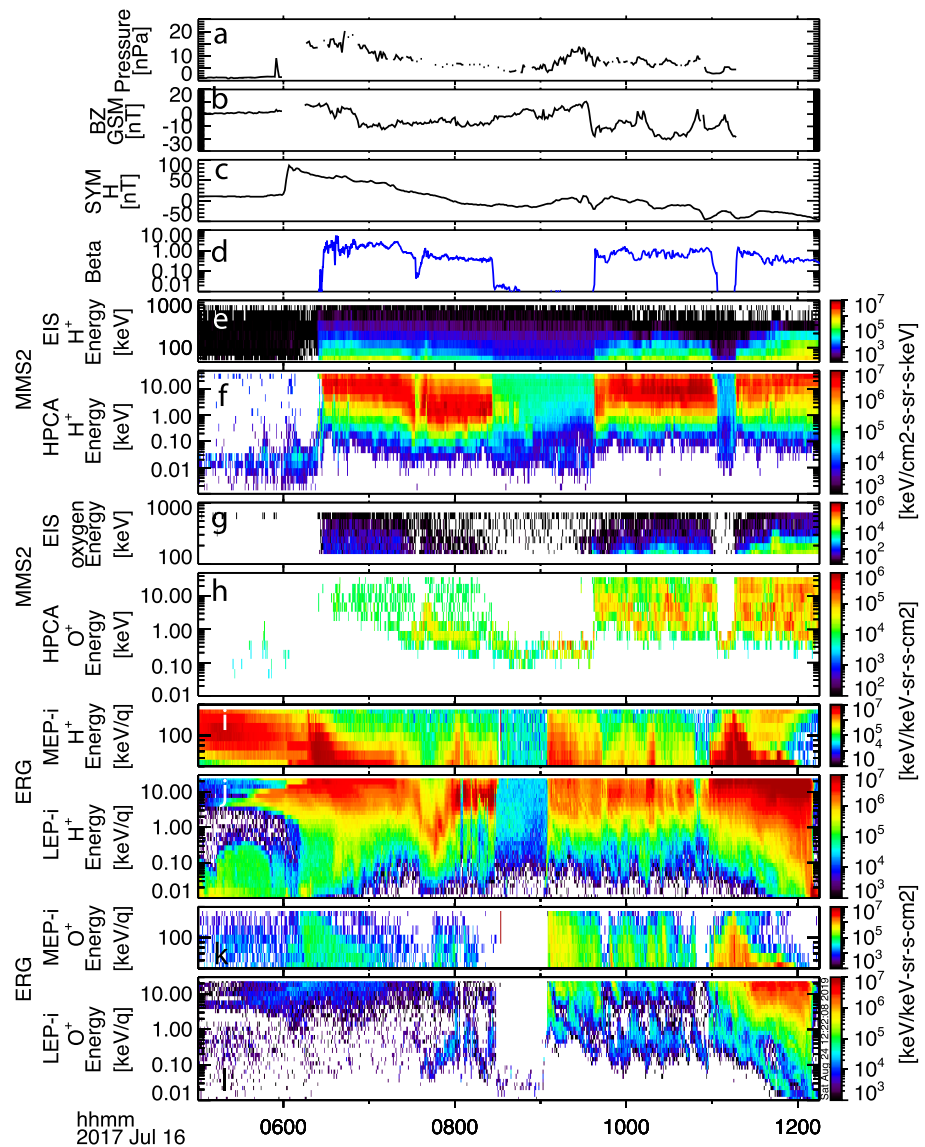


**Figure 2.** Data from 5:00 to 12:00 on 16 July 2017. (a and b) solar wind dynamic pressure and  $B_z$ , from the Omni data set; (c) SYM- $H$  index; (d) plasma beta from MMS2; (e and f)  $H^+$  omnidirectional energy flux from MMS2; (g and h)  $O^+$  omnidirectional energy flux, from MMS2; (i and j)  $H^+$  omnidirectional differential energy flux from ARG; and (k and l)  $O^+$  omnidirectional differential energy flux from ARG.

8:30, just a few minutes after MMS entered the lobe, with the  $H^+$  dropping out almost completely. Arase re-enters the plasma sheet at 9:05. After 11:00, the spacecraft moves inbound to perigee.

The final two panels show  $O^+$  from the Arase satellite. There is a small enhancement in the energetic  $O^+$  when the pressure pulse hits, followed by an injection, similar to that observed in the  $H^+$ . Then, as at the MMS spacecraft, a separate low-energy population is observed that continues as the spacecraft moves into the lobe. When the spacecraft re-enters the plasma sheet, two populations are evident: an energetic population, and at lower energies, a set of bursts that start at higher energies, and then decrease. Then, at 11:00, the spacecraft inbound pass toward perigee begins. During this time, there is a separate low-energy population that decreases in energy as the spacecraft moves earthward.

Figure 3 shows the lower energy (HPCA and LEPI)  $O^+$  data and magnetic field data for the time period 7:00 to 11:30. Figure 3a shows the magnetic field on MMS, indicating that MMS is north of the neutral sheet ( $B_x > 0$ ). Figures 3b and 3c show the MMS HPCA  $O^+$  energy spectra for two pitch angle ranges:  $0-90^\circ$ ,



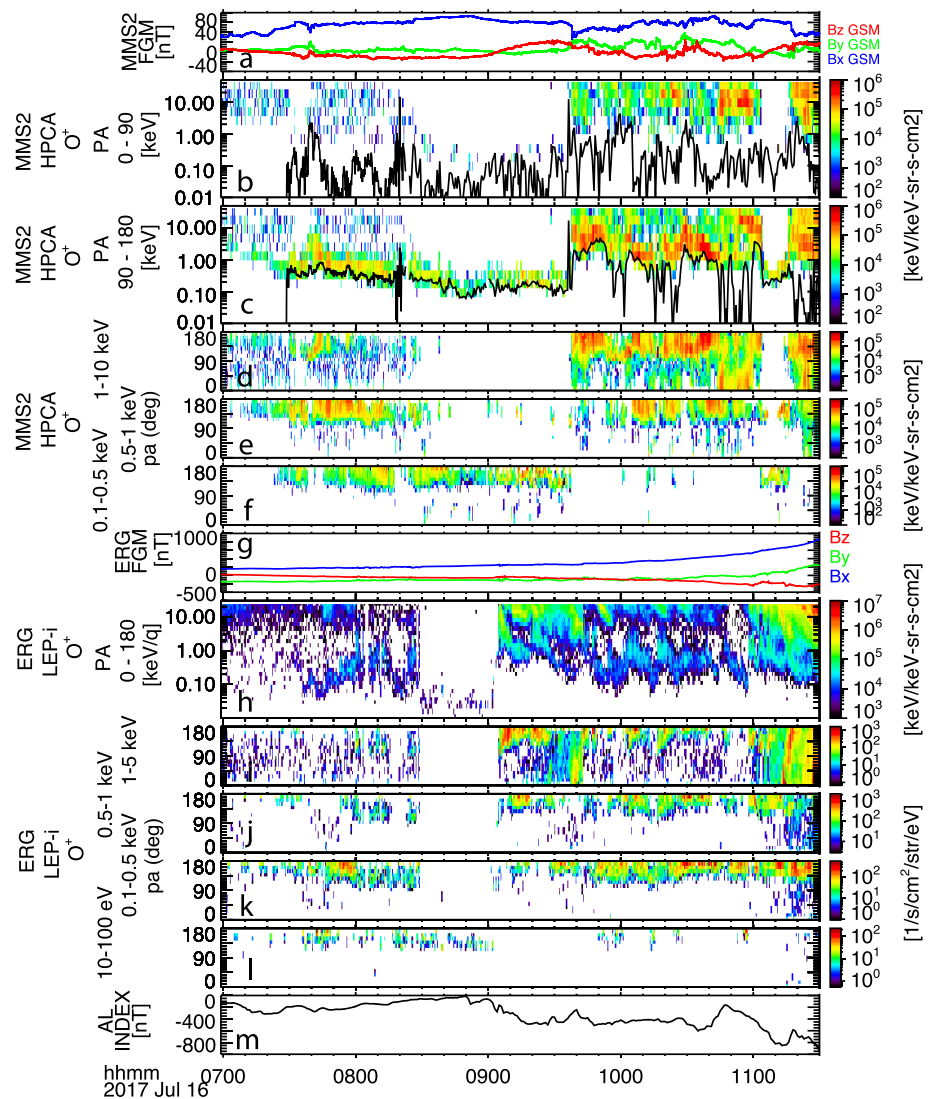


**Figure 3.**  $O^+$  and magnetometer data from 7:00 to 11:30 on 16 July 2017. (a) Magnetic field at MMS. (b) MMS  $O^+$  differential energy flux in the earthward (pitch angle  $0-90^\circ$ ) and energy corresponding to the perpendicular velocity. (c) MMS  $O^+$  differential energy flux in the tailward (pitch angle  $90-180^\circ$ ) direction and energy corresponding to the parallel velocity. MMS  $O^+$  pitch angle spectra for the energy ranges (d) 1–10 keV, (e) 0.5–1.0 keV, and (f) 0.1–0.5 keV. (g) Magnetic field at ERG. (h) ERG  $O^+$  omnidirectional flux. ERG  $O^+$  pitch angle spectra from the energy ranges (i) 1–5 keV, (j) 0.5–1.0 keV, (k) 0.1–0.5 keV, and (l) 10–100 eV. (m) AL index.

corresponding to earthward motion, and  $90-180^\circ$ , corresponding to tailward motion. Figures 3d–3f show the pitch angle distributions in three energy ranges, ordered from high to low energy. Figure 3g shows the magnetic field on Arase, and Figures 3h–3m show the Arase LEPi  $O^+$  energy spectrum, and the pitch angle distributions in four energy ranges, again ordered from high to low energy. Pitch angles are calculated in the spacecraft frame.

From 7:30 to 9:00, both spacecraft are first in the PSBL and then move into the lobe. The low-energy populations at the two spacecraft are observed almost simultaneously. The pitch angle distributions show that these particles are tailward moving, and narrow in both energy range and pitch angle range. However, the population observed at MMS is at a higher energy than the population at Arase. In the lobe ( $\sim 8:30$  to 9:00 UT), the population observed at MMS is at  $\sim 200$  eV, while the population observed simultaneously at Arase is at  $\sim 30$  eV. The black line in Figure 3b indicates the energy associated with the perpendicular  $O^+$  velocity (calculated as a moment of the distribution), while the line in Figure 3c indicates the energy associated with the parallel  $O^+$  velocity. The parallel velocity line closely follows the energy of the tailward moving population.

From 9:40 to 10:40, different behavior is observed at the two spacecraft. At the Arase spacecraft, there is a bursty population that shows a clear energy dispersion starting from  $\sim 1$  keV and decreasing to  $\sim 100$  eV. The bursty population is well separated from the higher-energy plasma sheet population. The pitch angle distributions indicate that this population is also tailward and close to field aligned.

Simultaneous with these observations, MMS also observes similar bursts. However, they are not as clear as on Arase because they are more energetic, and so there is not a clear gap between this population and the hot plasma sheet population, as there is for Arase. However, by separating the earthward from the tailward spectra, in Figures 3b and 3c, it can be more clearly seen that there is an additional tailward moving population that also shows energy dispersion. The line indicating the energy of the parallel component in Figure 3c shows the energy variation clearly. For example, there is one burst starting at 10:02, another smaller one at 10:18, and another at 10:28. This shows that the energy variations are predominantly in the parallel component. The variations in the perpendicular component, shown by the line in Figure 3b, do not follow the energy changes. The pitch angle distributions also indicate that these are tailward streaming ions. However, once again, MMS observes the ions at higher energies than Arase. At MMS the dispersed ions start at  $\sim 10$  keV, and go down to 1 keV. The bottom panel shows the *AL* index. The decrease in *AL* at 9:00, at the same time that the bursty ions are observed, indicates the association of these bursts with substorm activity. At 11:04, the MMS spacecraft again moves into the lobe. The low-energy monoenergetic population is still observed.

#### 4. Discussion

During the main phase of this storm, both the Arase satellite and the MMS satellite show signatures of two different populations of  $O^+$  entering the plasma sheet. The first population is observed in the lobe and then enters the plasma sheet through the PSBL. The second population is bursty with clear dispersion, indicating more direct access from a time-varying source. As discussed in section 1, it is well known that there are two dominant regions of energetic ion outflow, the dayside cusp and the nightside auroral region. Both are enhanced during storm times, and can provide outflow with energies close to the energies observed. Thus, a reasonable hypothesis would be that these two sources are the origin of the two populations.

To understand the characteristics of the ions from these two sources observed in the plasma sheet, it is important to understand the properties expected as a result of the transport. From both locations, the ion motion is a combination of parallel motion along the field, which is higher for higher-energy ions, and convective motion perpendicular to the field, which is the same for ions of all energies. Because the parallel velocity scales with the energy, while the perpendicular velocity does not, the ion trajectories are different for different energy ions. For cusp ions, as the magnetic field convects from the dayside over the polar cap and into the nightside lobes, the higher-energy ions travel further down the field than lower energy ions. Thus, the higher-energy cusp ions reach the PSBL further down the tail than lower energy ions. This dispersion of the ions is called the “velocity filter effect” or the “tail lobe ion spectrometer” (Candidi et al., 1988; Horwitz, 1986). Ions from the nightside aurora also move with a combination of field-aligned motion and convective perpendicular motion. Thus, this population can also exhibit spatial dispersion. As with the cusp ions, the spatial dispersion results because the field line is convecting toward the central plasma sheet as the  $O^+$  ions move up the field line. Thus, for ions from the nightside aurora, the lower energy ions will end up closer to the central plasma sheet at a given distance and closer to the Earth when they reach the neutral sheet than higher-energy ions. However, temporal dispersion can also occur. The temporal dispersion occurs because the auroral outflow is bursty, and higher energies will take less time to move up the field line. Nosé et al. (2016) modeled the transit time for  $O^+$  ions to reach  $15^\circ$  GMLAT at  $L = 6.6$ , and found a range from  $\sim 3$  min for 5 keV ions to 20 min for 100 eV ions, consistent with the temporal dispersion they observed.

Thus, qualitatively, the observations of Arase and MMS are consistent with the two sources. The ions observed in the lobe, coming in through the PSBL, are the cusp-source ions. As expected from the velocity filter effect, MMS, further down the tail, observes the ions at higher energies than Arase, located closer to the Earth. The bursty population observed in the plasma sheet shows the characteristics expected from the nightside auroral source. The temporal dispersion comes from the time that it takes for different energy ions to make it up the field line, as shown by Nosé et al. (2016). But spatial dispersion also plays a role. The strongest nightside auroral outflow occurs at the polar cap boundary, which maps to the plasma sheet



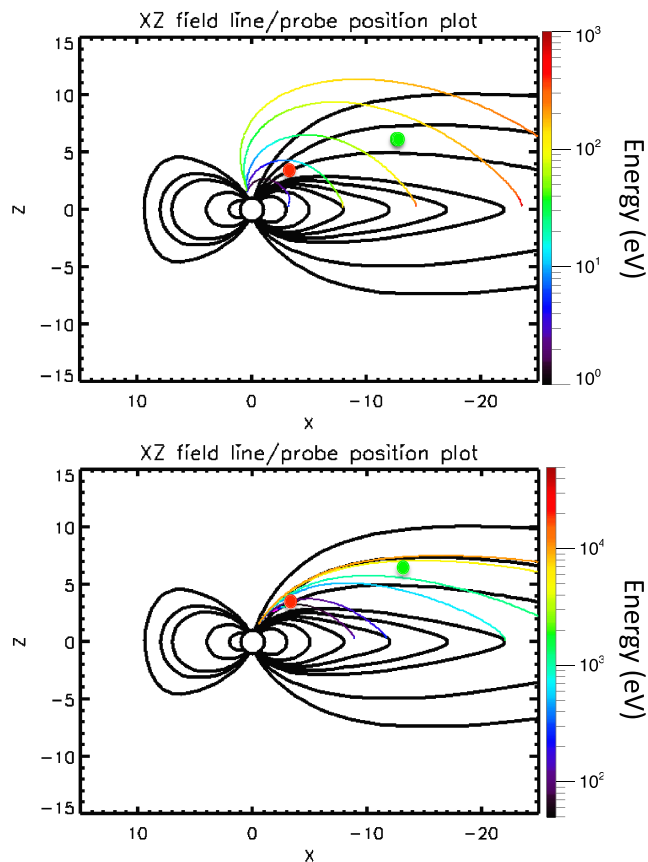


**Figure 4.** (a) Ion trajectories from 75 latitude, 13.0 MLT, 4,000 km. Initial energies are 3, 5, 10, 25, and 50 eV at 100° pitch angle. The trajectory color indicates the particle energy. (b) Ion trajectories from 70 latitude, 22.6 MLT, 4,000 km. Initial energies are 50, 100, 500, 1,000, 5,000, and 10,000 eV. In both plots the red dot indicates the ERG location and the green dot indicates the MMS-2 location. Note that the color bar ranges are different in the two plots.

boundary layer (Tung et al., 2001). However, because of the convection toward the neutral sheet, only the fastest ions will stay close to the boundary and make it further down the tail. The slower ions will be observed closer in. The fact that MMS, located further down the tail, only observes the higher-energy ions, from 1 to 10 keV while the closer in Arase spacecraft usually observes the lower energy ions, from 0.1 to 1 keV, is consistent with this spatial dispersion. Thus, the combination of MMS and Arase observations show both the temporal dispersion, in the time delay of the different energies in each individual burst, and spatial dispersion in the different energies that are able to reach MMS and Arase.

In order to test whether the qualitative understanding of these observations also holds quantitatively, we have modeled the trajectories of ions from the dayside cusp and nightside auroral region using a Tsyganenko, 1989 magnetic field, with no dipole tilt, for  $K_p = 6$  combined with a Volland (1978) electric field, using the particle tracing code of Delcourt (1985) and Sauvaud and Delcourt (1987). To model this main-phase storm time event, a cross-polar-cap potential of 150 kV is assumed, which is a reasonable storm-time value (Hairston et al., 2005). The transport of the ions from the two sources to the plasma sheet is illustrated in Figure 4. For the cusp, in Figure 4a, ions are started from 4,000 km, and 75° latitude at 13:00 MLT with energies of 3, 5, 10, 25, and 50 eV at 100° pitch angle. This is to simulate ions perpendicularly accelerated in the cusp region. The energy of the particles is indicated by the color of the trajectory. As has been shown previously (e.g., Cladis, 1986; Delcourt et al., 1993; Kitamura et al., 2010; Yau et al., 2012), in addition to the dispersion by the velocity filter effect, there is also significant acceleration of the ions along the trajectory from the cusp. This is due to centrifugal acceleration along the field as the field line convects over the polar cap. Thus, the cusp ions that start at energies from 5 to 50 eV end up in the lobe adjacent to the plasma sheet with energies ranging from 30 to 300 eV, consistent with the energies observed in the lobe by MMS and Arase. In addition, the ion energies continue to increase as the ions move toward the central plasma sheet, also as observed in the data. The ion energies when they reach the neutral sheet are 500 eV to 1 keV between 10 and 20 Re, again, consistent

with the observations. The spatial dispersion of the trajectories of different energy ions is clearly seen, explaining the different energies observed at Arase and MMS in the lobe.

Figure 4b shows the trajectories of nightside auroral ions in the same magnetic and electric field configuration. Particles are started from 4,000 km with a pitch angle of 100°, from MLT 22.6 hr and 70° latitude, simulating the nightside aurora. Trajectories are shown for ions with initial energies of 50, 100, 500, 1,000, 5,000, and 10,000 eV. In contrast to the cusp, there is very little acceleration along the trajectory due to the straighter paths, particularly for the high-energy ions. Thus, the ions that are observed in the plasma sheet boundary were accelerated almost to these energies in the auroral regions. Again, the spatial dispersion is clear. High-energy ions (5,000 and 10,000 eV) remain very close to the plasma sheet boundary layer, while lower energy ions are convected toward the neutral sheet. Thus, only high-energy ions from this source can reach the MMS location, while lower energy ions can be observed at Arase. If Arase is close to the boundary, it should also see the highest-energy ions. Figure 3g shows that this is the case. At 9:03, when Arase enters the plasma sheet, the first dispersed burst is observed, and it starts at ~10 keV. The pitch angle distribution in Figure 3h shows that just as Arase enters the plasma sheet, the pitch angle is perpendicular, but a few minutes later it is parallel, and the energy is still high, and then decreases. It is later, when Arase is further from the boundary, that it only sees the lower energies.

To determine if the energy dispersion is consistent with a time-of-flight effect, Table 1a gives the time for the ions from the nightside aurora to reach 5 Re, the location of the Arase satellite, in the simulation. Ions of 100

**Table 1**  
*Travel Times of Ions From the Source Region to the Tail*

a) Travel from the nightside auroral source region

Source	Initial energy (eV)	Time to 5 re (min)	Time to 12 re (min)
Nightside	100	13.12	
Nightside	500	5.73	16.24
Nightside	1000	4.08	11.36
Nightside	5000	1.83	5.07
Nightside	10000	1.3	3.06

b) Travel from the dayside cusp region

Source	Initial energy (eV)	Time to neutral sheet (min)
Cusp	3	174
Cusp	5	124.9
Cusp	10	117.9
Cusp	25	113.8
Cusp	50	110

eV take 13.1 min, while ions of 1 keV take only 4.1 min, so we expect the time of the energy dispersion from 1 keV to 100 eV to be a little over 9 min. This timing agrees with the observed dispersion. For example one burst goes from ~10:04 to 10:13, while the next one goes from 10:16 to 10:25. Similar dispersion is also expected at MMS. MMS is at ~12 Re during this time. Table 1 also shows the time for the ions to reach 12 Re. From the flight times, we would expect about an 8-min difference between 10 and 1 keV. This is on the order of the dispersion observed in the burst, for example, from 10:30 to 10:40. However, in general, the dispersion is less clear at the MMS location. This is likely because there is field line motion at the boundary, indicated by MMS moving in and out of the lobe, and this motion will change the field line that maps to MMS, bringing a different ion energy to the spacecraft. This type of motion makes it more difficult to discern the temporal dispersion.

Finally, Table 1b gives the amount of time it takes the cusp ions to reach the neutral sheet. The ions from 5 eV and above take around

2 hr to reach neutral sheet. Thus, it is quite reasonable that these ions can reach the plasma sheet during the main phase of a storm and get injected into the ring current.

The exact trajectories will of course depend on the cross polar cap potential. While a weaker polar cap potential will increase the distance and time and decrease the energies at which the ions reach the neutral sheet, the relative dispersion of ions by their velocity will remain the same. As a measure of the sensitivity, for the 10-eV ion from the cusp, for example, a change in the potential from 150 to 100 kV would increase the neutral sheet crossing distance from 15 to 20 Re and decrease the energy at the neutral sheet from 800 to 600 eV.

An alternative possibility for the tailward streaming populations observed at MMS is that these ions are cusp-origin ions, accelerated in the PSBL, as suggested by Lindstedt et al. (2010) or Lennartsson (2003). As has often been observed, the energy of the cusp ions increase as they enter the plasma sheet and move toward the neutral sheet. However, the mechanisms proposed for this would accelerate the ions in the perpendicular direction. The argument against this is that, as shown in Figure 3b, the changes in the tailward streaming ions are predominantly in the parallel component, indicating that they have been accelerated at a location closer to the Earth and are just reaching the spacecraft, rather than that they are a locally accelerated population. There is no doubt that some perpendicular acceleration does occur along the transport path. As noted, some perpendicular motion was observed at Arase. In addition, if the ions observed at MMS were only accelerated in the auroral acceleration region, the mirror force would make the pitch angle distribution much narrower than observed. Another possibility is that the tailward ions at MMS are accelerated through reconnection. While reconnection would normally be tailward of the MMS location, leading to earthward flows, reconnection is sometimes observed inside 16 Re (Genestreti et al., 2014). Thus, it cannot be excluded that tailward  $O^+$  was accelerated through reconnection. But the combination of the Arase and MMS observations of the bursty field-aligned populations strongly points to the nightside aurora as the source.

## 5. Conclusions

In this paper we have shown that during the main phase of a storm, ions from both the nightside auroral sources and the cusp are observed entering the plasma sheet in the  $L = 6$  to 15 Re region. The entering cusp ions tend to be at lower energies in the lobe, and their energy increases as they move toward the neutral sheet. The nightside aurora brings ions of up to 10 keV into the plasma sheet boundary layer. Lower energy ions are observed earthward and closer to the neutral sheet. Thus,  $O^+$  from both sources are entering the plasma sheet during the main phase of a storm.

In some cases, the two sources are easy to distinguish. The low-energy (20–200 eV) ions in the lobe are clearly not from the nightside aurora, and when these ions are observed clearly coming into the plasma sheet through the boundary layer, their source is clear. On the other hand, the 10-keV tailward beam in the 10–20-Re plasma sheet boundary layer is very unlikely to come from the cusp, and so more likely indicates an

auroral source. But somewhat surprisingly, despite the difference in acceleration along their paths, both sources can provide ~1-keV ions to the 10–20-Re neutral sheet. Thus, in cases when there is not a clear dispersed burst or a clear contiguous connection to the lobe, the source can be ambiguous.

The importance of the two sources may vary from event to event, and may also change with time during the storm. In some cases, such as the event discussed by Kistler et al. (2016), a pressure pulse hit the Earth 8 hr before the main phase of the storm. Because of this, the  $O^+$  in the plasma sheet increased significantly before the storm occurred, likely due to cusp outflow, so that the plasma sheet was already full of  $O^+$  when the storm began. The strongly enhanced AE and the bursty nightside outflow was only observed during the main phase. For the storm discussed in this paper, the pressure pulse occurs only approximately half an hour before the southward turning of the field, so there was no preconditioning of the plasma sheet, and both sources contributed strongly during the main phase.

The fact that such low-energy cusp outflow is able to reach the plasma sheet in reasonably short time scales means that a significant fraction of the cusp outflow may reach the plasma sheet during storms. Kitamura et al. (2010) reached a similar conclusion. Akebono measured high fluxes of very low energy  $O^+$  (<10 eV) originating in the cleft ion fountain. Trajectory calculations similarly showed that these ions were likely to reach the plasma sheet and from there into the ring current under strong convection. Similarly, Nakayama et al. (2017) simulated ions from both the dayside polar regions and the nightside aurora and found that the dayside ions were more likely to reach the plasma sheet, get accelerated and reach the ring current, while the contribution from the nightside aurora is small.

However, this event does show that the high-energy (>1 keV) portion of the nightside auroral outflow can get far enough down the tail that it will reach a thin neutral sheet and get scattered, similar to the cusp ions. In fact, the two populations reach the midtail plasma sheet with about the same energies. Both can bring ~1-keV ions into the 15–20-Re neutral sheet, where their further trajectories will be similar. Thus, determining which source has the greater contribution needs to be done with a careful analysis of the spatial and temporal extent of the outflow during the storm, and with observations of the ions on their transport paths to the plasma sheet.

## Acknowledgments

Work at UNH was supported by NASA under grant 80NSSC17K0643. Work by L.M.K. at Nagoya was supported by ISEE, Nagoya University. A part of this work was supported by JSPS Grants-in-Aid for Scientific Research (15H05747, 15H05815, 16H06286, 17H00728). MMS data were obtained from the Science Data Center (SDC) at <https://lasp.colorado.edu/mms/sdc/>. Science data of the Arase (ERG) satellite were obtained from the ERG Science Center (ERG-SC) operated by ISAS/JAXA and ISEE/Nagoya University (<https://ergsc.isee.nagoya-u.ac.jp/index.shtml.en>). The present study analyzed LEPi Level-2 v03.00, ERG MGF Level-2 v01.01 data, and MEPi Level-2 v01.03 (omni) and v01.01(TOF) data. The Arase data will be publically available via ERG-SC on a project-agreed schedule. Part of the work of Y.M. and T.H. was funded by the ERG-SC. The Space Physics Environmental Data Analysis Software (SPEDAS) package was used to process the ERG and MMS data. Solar wind plasma and IMF data and SYM-H indices were obtained from <http://omniweb.gsfc.nasa.gov>.

## References

- Andersson, L., Peterson, W. K., & McBryde, K. M. (2005). Estimates of the suprathermal  $O^+$  outflow characteristic energy and relative location in the auroral oval. *Geophysical Research Letters*, 32(9), 09104. <https://doi.org/10.1029/2004GL021434>
- Asamura, K., Kazama, Y., Yokota, S., Kasahara, S., & Miyoshi, Y. (2018). Low-energy particle experiments-ion mass analyzer (LEPi) onboard the ERG (Arase) satellite. *Earth, Planets and Space*, 70(1), 70. <https://doi.org/10.1186/s40623-018-0846-0>
- Candidi, M., Orsini, S., & Formisano, V. (1982). The properties of ionospheric  $O^+$  ions as observed in the magnetotail boundary layer and northern plasma lobe. *Journal of Geophysical Research*, 87(A11), 9097–9106. <https://doi.org/10.1029/JA087iA11p09097>
- Candidi, M., Orsini, S., & Horwitz, J. L. (1988). The tail lobe ion spectrometer - theory and observations. *Journal of Geophysical Research*, 93(A12), 14,401–14,409. <https://doi.org/10.1029/JA093iA12p14401>
- Chappell, C. R., Huddleston, M. M., Moore, T. E., Giles, B. L., & Delcourt, D. C. (2008). Observations of the warm plasma cloak and an explanation of its formation in the magnetosphere. *Journal of Geophysical Research*, 113(A9), A09206. <https://doi.org/10.1029/2007JA012945>
- Cladis, J. B. (1986). Parallel acceleration and transport of ions from polar ionosphere to plasma sheet. *Geophysical Research Letters* (ISSN 0094-8276), 13, 893–896. [https://doi.org/10.1029/GL013i009p00893\\_9](https://doi.org/10.1029/GL013i009p00893_9)
- Collin, H. L., Peterson, W. K., & Shelley, E. G. (1987). Solar cycle variation of some mass dependent characteristics of upflowing beams of terrestrial ions. *Journal of Geophysical Research*, 92(A5), 4757–4762. <https://doi.org/10.1029/JA092iA05p04757>
- Cully, C. M., Donovan, E. F., Yau, A. W., & Arkos, G. G. (2003). Akebono/Suprathermal mass spectrometer observations of low-energy ion outflow: Dependence on magnetic activity and solar wind conditions. *Journal of Geophysical Research*, 108(A2), 1093. <https://doi.org/10.1029/2001JA009200>
- Daglis, I. A., & Axford, W. I. (1996). Fast ionospheric response to enhanced activity in geospace: Ion feeding of the inner magnetotail. *Journal of Geophysical Research*, 101(A3), 5047–5065. <https://doi.org/10.1029/95JA02592>
- Delcourt, D. (1985). *Circulation Des Ions Ionosphériques Suprathermiques Dans la Magnétosphère Terrestre, these de Doctorat de Spécialité* 3256. Toulouse, France: Univ. Toulouse.
- Delcourt, D. C., Giles, B. L., Chappell, C. R., & Moore, T. E. (1988). Low-energy bouncing ions in the magnetosphere - a three-dimensional numerical study of dynamics explorer 1 data. *Journal of Geophysical Research*, 93(A3), 1859–1870. <https://doi.org/10.1029/JA093iA03p01859>
- Delcourt, D. C., Sauvaud, J. A., & Moore, T. E. (1993). Polar wind ion dynamics in the magnetotail. *Journal of Geophysical Research*, 98(A6), 9155–9169. <https://doi.org/10.1029/93JA00301>
- Fuselier, S. A., Collin, H. L., Ghielmetti, A. G., Clafin, E. S., Moore, T. E., Collier, M. R., et al. (2002). Localized ion outflow in response to a solar wind pressure pulse. *Journal of Geophysical Research*, 107(A8), SMP 26-1–SMP 26-9. <https://doi.org/10.1029/2001JA000297>
- Gazey, N. G. J., Lockwood, M., Grande, M., Perry, C. H., Smith, P. N., Coles, S., et al. (1996). EISCAT/CRRES observations: Nightside ionospheric ion outflow and oxygen-rich substorm injections. *Annales Geophysicae*, 14(10), 1032–1043. <https://doi.org/10.1007/s00585-996-1032-4>

- Genestreti, K. J., Fuselier, S. A., Goldstein, J., Nagai, T., & Eastwood, J. P. (2014). The location and rate of occurrence of near-earth magnetotail reconnection as observed by cluster and Geotail. *Journal of Atmospheric and Solar-Terrestrial Physics*, 121, 98–109. <https://doi.org/10.1016/j.jastp.2014.10.005>
- Hairston, M. R., Drake, K. A., & Skoug, R. (2005). Saturation of the ionospheric polar cap potential during the October–November 2003 superstorms. *Journal of Geophysical Research*, 110(A9), A09S26. <https://doi.org/10.1029/2004JA010864>
- Hirahara, M., Nakamura, M., Terasawa, T., Mukai, T., Saito, Y., Yamamoto, T., et al. (1994). Acceleration and heating of cold ion beams in the plasma sheet boundary layer observed with GEOTAIL. *Geophysical Research Letters* (ISSN 0094-8276), 21, 3003–3006. <https://doi.org/10.1029/94GL02109>, 25
- Horwitz, J. L. (1986). The tail lobe ion spectrometer. *Journal of Geophysical Research*, 91(A5), 5689–5699. <https://doi.org/10.1029/JA091iA05p05689>
- Kistler, L. M., Mouikis, C. G., Klecker, B., & Dandouras, I. (2010). Cusp as a source for oxygen in the plasma sheet during geomagnetic storms. *Journal of Geophysical Research*, 115(A3), 03209. <https://doi.org/10.1029/2009JA014838>
- Kistler, L. M., Mouikis, C. G., Spence, H. E., Menz, A. M., Skoug, R. M., Funsten, H. O., et al. (2016). The source of O<sup>+</sup> in the storm time ring current. *Journal of Geophysical Research: Space Physics*, 121, 5333–5349. <https://doi.org/10.1002/2015JA022204>
- Kitamura, N., Nishimura, Y., Ono, T., Ebihara, Y., Terada, N., Shinbori, A., et al. (2010). Observations of very-low-energy (<10 eV) ion outflows dominated by O<sup>+</sup> ions in the region of enhanced electron density in the polar cap magnetosphere during geomagnetic storms. *Journal of Geophysical Research*, 115(A11), A00J06. <https://doi.org/10.1029/2010JA015601>
- Lennartsson, O. W. (2003). In situ polar observation of transverse cold-ion acceleration: Evidence that electric field generation is a hot-ion finite gyroradii effect. *Journal of Geophysical Research*, 108(A4), 1152. <https://doi.org/10.1029/2002JA009663>
- Liao, J., Kistler, L. M., Mouikis, C. G., Klecker, B., Dandouras, I., & Zhang, J.-C. (2010). Statistical study of O<sup>+</sup> transport from the cusp to the lobes with cluster CODIF data. *Journal of Geophysical Research*, 115(A12), A00J15. <https://doi.org/10.1029/2010JA015613>
- Liemohn, M. W., Moore, T. E., Craven, P. D., Maddox, W., Nagy, A. F., & Kozyra, J. U. (2005). Occurrence statistics of cold, streaming ions in the near-earth magnetotail: Survey of polar-TIDE observations. *Journal of Geophysical Research*, 110(A7), A07211. <https://doi.org/10.1029/2004JA010801>
- Lindstedt, T., Khotyaintsev, Y. V., Vaivads, A., André, M., Nilsson, H., & Waara, M. (2010). Oxygen energization by localized perpendicular electric fields at the cusp boundary. *Geophysical Research Letters*, 37(9), 9103, L09103. <https://doi.org/10.1029/2010GL043117>
- Lund, E. J., Nowrouzi, N., Kistler, L. M., Cai, X., & Frey, H. U. (2018). On the role of ionospheric ions in Sawtooth events. *Journal of Geophysical Research: Space Physics*, 123(1), 665–684. <https://doi.org/10.1002/2017JA024378>
- Maggiolo, R. (2016). Auroral arcs and ion outflow. In Y. Zhang & L. J. Paxton (Eds.), *Auroral Dynamics and Space Weather*, *Geophysical Monograph* (Vol. 215, pp. 39–58). Hoboken, NJ USA: John Wiley & Sons, Inc. <https://doi.org/10.1002/9781118978719.ch4>
- Maggiolo, R., & Kistler, L. M. (2014). Spatial variation in the plasma sheet composition: Dependence on geomagnetic and solar activity. *Journal of Geophysical Research: Space Physics*, 119, 2836–2857. <https://doi.org/10.1002/2013JA019517>
- Matsuoka, A., Teramoto, M., Nomura, R., Nosé, M., Fujimoto, A., Tanaka, Y., et al. (2018). The Arase (ERG) magnetic field investigation. *Earth, Planets and Space*, 70(1), 43. <https://doi.org/10.1186/s40623-018-0800-1>
- Mauk, B. H., Blake, J. B., Baker, D. N., Clemmons, J. H., Reeves, G. D., Spence, H. E., et al. (2016). The energetic particle detector (EPD) investigation and the energetic ion spectrometer (EIS) for the Magnetospheric Multiscale (MMS) Mission. *Space Science Reviews*, 199(1–4), 471–514. <https://doi.org/10.1007/s11214-014-0055-5>
- Miyoshi, Y., Shinohara, I., Takashima, T., Asamura, K., Higashio, N., Mitani, T., et al. (2018). Geospace exploration project ERG. *Earth*, 70(1), 1–13. <https://doi.org/10.1186/s40623-018-0862-0>
- Möbius, E., Tang, L., Kistler, L. M., Popecki, M., Lund, E. J., Klumpar, D., et al. (1998). Species dependent energies in upward directed ion beams over auroral arcs as observed with FAST TEAMS. *Geophysical Research Letters*, 25(12), 2029–2032. <https://doi.org/10.1029/98GL00381>
- Moore, T. E., Peterson, W. K., Russell, C. T., Chandler, M. O., Collier, M. R., Collin, H. L., et al. (1999). Ionospheric mass ejection in response to a CME. *Geophysical Research Letters*, 26(15), 2339–2342. <https://doi.org/10.1029/1999GL900456>
- Mukai, T., Hirahara, M., Machida, S., Saito, Y., Terasawa, T., & Nishida, A. (1994). Geotail observation of cold ion streams in the medium distance magnetotail lobe in the course of a substorm. *Geophysical Research Letters* (ISSN 0094-8276), 21, 1023–1026. <https://doi.org/10.1029/93GL02424>, 11
- Nakayama, Y., Ebihara, Y., Fok, M.-C., & Tanaka, T. (2017). Impact of substorm time O<sup>+</sup> outflow on ring current enhancement. *Journal of Geophysical Research: Space Physics*, 122, 6304–6317. <https://doi.org/10.1002/2016JA023766>
- Nosé, M., Keika, K., Kletzing, C. A., Spence, H. E., Smith, C. W., MacDowall, R. J., et al. (2016). Van Allen probes observations of magnetic field dipolarization and its associated O<sup>+</sup> flux variations in the inner magnetosphere at L. *Journal of Geophysical Research: Space Physics*, 121, 7572–7589. <https://doi.org/10.1002/2016JA022549>
- Orsini, S., Candidi, M., Stockholm, M., & Balsiger, H. (1990). Injection of ionospheric ions into the plasma sheet. *Journal of Geophysical Research*, 95(A6), 7915–7928. <https://doi.org/10.1029/JA095iA06p07915>
- Peterson, W. K., Andersson, L., Callahan, B. C., Collin, H. L., Scudder, J. D., & Yau, A. W. (2008). Solar-minimum quiet time ion energization and outflow in dynamic boundary related coordinates. *Journal of Geophysical Research*, 113(A7), 07222. <https://doi.org/10.1029/2008JA013059>
- Sauvaud, J. A., & Delcourt, D. (1987). A numerical study of suprathermal ionospheric ion trajectories in three-dimensional electric and magnetic field models. *Journal of Geophysical Research*, 92(A6), 5873–5884. <https://doi.org/10.1029/JA092iA06p05873>
- Sauvaud, J. A., Louarn, P., Fruit, G., Stenuit, H., Vallat, C., Dandouras, J., et al. (2004). Case studies of the dynamics of ionospheric ions in the Earth's magnetotail. *Journal of Geophysical Research*, 109(A1), 01212. <https://doi.org/10.1029/2003JA009996>
- Tsyganenko, N. A. (1989). A magnetospheric magnetic field model with a warped tail current sheet. *Planetary and Space Science* (ISSN 0032-0633), 37, 5–20. [https://doi.org/10.1016/0032-0633\(89\)90066-4](https://doi.org/10.1016/0032-0633(89)90066-4), 1
- Tung, Y. K., Carlson, C. W., McFadden, J. P., Klumpar, D. M., Parks, G. K., Peria, W. J., & Liou, K. (2001). Auroral polar cap boundary ion conic outflow observed on FAST. *Journal of Geophysical Research*, 106(A3), 3603–3614. <https://doi.org/10.1029/2000JA900115>
- Volland, H. (1978). A model of the magnetospheric electric convection field. *Journal of Geophysical Research*, 83(A6), 2695–2699. <https://doi.org/10.1029/JA083iA06p02695>
- Williams, D. J. (1981). Ring current composition and sources - An update. *Planetary and Space Science*, 29, 1195–1203. [https://doi.org/10.1016/0032-0633\(81\)90124-0](https://doi.org/10.1016/0032-0633(81)90124-0)
- Wilson, G. R., Ober, D. M., Germany, G. A., & Lund, E. J. (2004). Nightside auroral zone and polar cap ion outflow as a function of substorm size and phase. *Journal of Geophysical Research*, 109(A2), A02206. <https://doi.org/10.1029/2003JA009835>

- Yau, A. W., Howarth, A., Peterson, W. K., & Abe, T. (2012). Transport of thermal-energy ionospheric oxygen (O<sup>+</sup>) ions between the ionosphere and the plasma sheet and ring current at quiet times preceding magnetic storms. *Journal of Geophysical Research*, 117(A7), 7215, A07215. <https://doi.org/10.1029/2012JA017803>
- Yokota, S., Kasahara, S., Mitani, T., Asamura, K., Hirahara, M., Takashima, T., et al. (2017). Medium-energy particle experiments-ion mass analyzer (MEP-i) onboard ERG (Arase). *Earth, Planets and Space*, 69(1), 172. <https://doi.org/10.1186/s40623-017-0754-8>
- Young, D. T., Burch, J. L., Gomez, R. G., De Los Santos, A., Miller, G. P., Wilson, P., et al. (2014). Hot plasma composition analyzer for the Magnetospheric Multiscale Mission. *Space Science Reviews*, 199(1-4), 407–470. <https://doi.org/10.1007/s11214-014-0119-6>